Self-Supporting Uncooled Infrared Microbolometers With Low-Thermal Mass

Mahmoud Almasri, *Student Member, IEEE*, Donald P. Butler, *Senior Member, IEEE*, and Zeynep Çelik-Butler, *Senior Member, IEEE*

***Abstract*—A new micromachined microbolometer array structure is presented that utilizes a self-supporting semiconducting yttrium barium copper oxide (Y–Ba–Cu–O) thin film thermometer. The Y–Ba–Cu–O thermometer is held above the substrate only by the electrode arms without the need of any underlying supporting membrane. This represents a significant improvement in the state-of-the-art for microbolometers by eliminating the thermal mass associated with the supporting membrane. The reduced thermal mass permits lowering the thermal conductance to the substrate to obtain increased responsivity or having a shorter thermal time constant to allow for higher frame rate camera. The simple structure does not suffer from warping problems associated with stress imbalances in multilayer microbolometer structures that utilize a supporting membrane such as Si_3N_4. Devices were fabricated by growing Y–Ba–Cu–O films on a conventional polyimide sacrificial layer mesa. Subsequent etching of the sacrificial layer provides the air gap that thermally isolates the microbolometer. Y–Ba–Cu–O possesses a relatively high temperature coefficient of resistance of 3.1%/K at room temperature. The 400-nm-thick Y–Ba–Cu–O film exhibited absorptivity of about 30%. The responsivity and detectivity approached 10^4 V/W and 10^8 cm $Hz^{1/2}$/W to filtered blackbody infrared (IR) radiation covering the 2.5 to 13.5 μm band. This extrapolates to noise equivalent temperature difference (NETD) less than 100 mK. The micromachining techniques employed are post-complementary metal–oxide–semiconductor (CMOS) compatible, allowing for the fabrication of focal plane arrays for IR cameras. [649]**

***Index Terms*—Microbolometers, micromachining, uncooled infrared detection, yttrium barium copper oxide.**

I. Introduction

UNCOOLED infrared detector technology has attracted considerable interest due to the wide range of applications at low cost. Infrared imaging systems are used for drivers' aid, security, fire detection, search and rescue, manufacturing, military, and medical applications [1]–[4]. Thermal detectors exhibit a change in a measurable electrical property that accompanies a change in temperature of the sensitive element caused by absorption of IR radiation. The three primary types of thermal detectors are microbolometers, pyroelectric, and thermocouple detectors. Thermal detectors can operate at room temperature allowing for relatively low cost, reliable detection systems in the spectral range from 1 to 100 μm [5]–[9]. In the case of a microbolometer, the temperature change causes the electrical resistance to change, which is the parameter that is detected. Micromachining techniques are used to suspend the thermometer above the substrate in a bridge structure to minimize the heat lost by thermal conduction to the substrate. This allows the thermometer to integrate the radiant energy and produce large response. However, the decrease in thermal conductance slows the detector response time by producing a corresponding increase in the thermal time constant. To obtain near background radiation limited performance while maintaining a 30 Hz frame rate requires detector bridges with very low thermal mass. This paper describes self-supporting Y–Ba–Cu–O microbolometers with very low thermal mass. Several microbolometers based on bulk and surface micromachining have been designed. These microbolometers make use of a micromachined bridge structure for mechanical support and chemical passivation. Traditionally, they have been made of a thick layer of silicon nitride [2], silicon dioxide [10] or silicon oxinitride [11]. The sensing thermometer is deposited on top of the microbridge. Several materials have been used as the thermometer such as VO_x [2], [8], poly-Si–Ge [12], [13], or metal resistors such as, titanium [11], and niobium [14]. A wide variety of sacrificial layers can be employed in micromachining. Popular sacrificial layers employed today are silicon dioxide/quartz, polysilicon [10], or polyimide [13]. The sacrificial layer is used to suspend the detector structure above the substrate. There is a growing preference for sacrificial layers that can be dry etched to prevent hydrostatic stiction.

The thermal mass and the thermal mass per unit area of the 200-Å-thick platinum bolometers on 3000- to 5000-Å-thick SiN_x membranes were measured to be 1.7×10^{-9} J/K and 6.9×10^{-5} J/K-cm^2, respectively [15]. The thermal mass and thermal mass per unit area for a 500-Å-thick VO_x microbolometer on 5000-Å thick SiN_x was less than 1×10^{-9} J/K and 4×10^{-5} J/K-cm^2, respectively [8], [16]. The thermal mass and thermal mass per unit area for a 5000-Å-thick poly-SiGe microbolometer with a 1000 Å SiN_x absorber layer was observed to be 6.4×10^{-9} J/K and 2.56×10^{-4} J/K-cm^2, respectively [13]. In the latter work, the poly-Si–Ge bolometers were self-supporting without the use of any bridge material as the detectors described in this work. However, due to thick layer of IR sensitive material, self-standing poly-SiGe microbolometers could not achieve any lower thermal mass than their counterparts fabricated on a microbridge. In this work, we describe a method by which self-supporting 4000 Å Y–Ba–Cu–O microbolometers are built yielding $C \sim 3.5 \times 10^{-10}$ W/K or $c = 2.19 \times 10^{-5}$ J/K-cm^2.

Manuscript received November 11, 2000; revised March 30, 2001. This work was supported by the National Science Foundation (ECS-9800062), Army Research Office (38673PH), and NASA (NAS1-99100). Subject Editor D. P. Butler.

The authors are with the (e-mail: dpb@engr.smu.edu).

Publisher Item Identifier S 1057-7157(01)05550-0.

The performance of a microbolometer is characterized by certain figures of merit such as temperature coefficient of resistance, TCR, responsivity, R_v, and detectivity, D^*.

The voltage responsivity, R_v, of the detector is defined as the output signal divided by the input radiant power falling on the detector

$$R_V = \frac{I_b R \beta \eta}{G(1+\omega^2 \tau_{th}^2)^{1/2}} \tag{1}$$

where

- I_b bias current;
- R bolometer resistance;
- η fraction of the incident radiation absorbed;
- G total thermal conductance to the substrate (heat sink), which is usually dominated by the thermal conductance of the support structure;
- ω radiation modulation frequency;
- τ thermal response time, defined by the ratio of the device's thermal mass to its thermal conductance, C/G;
- β temperature coefficient of resistance (TCR).

The TCR is a measure of how rapidly the resistance of a material responds to a change in temperature

$$\beta = \frac{1}{R}\frac{dR}{dT}. \tag{2}$$

The thermal conduction through the electrode arms should not be made as small as possible without consideration of the response time requirement. Since most of the detector applications are imaging which requires at least a 30-Hz frame rate or 5-ms response time, in order to satisfy the high speed and sensitivity, the thermal mass of the detector needs to be as small as possible.

The electrical noise is important in determining the performance of an infrared detector. The detectivity D^* is a figure of merit that measures the signal to noise ratio and normalizes the performance of the detector with respect to the detector size

$$D^* = \frac{R_V \sqrt{\Delta f A}}{\Delta V_n} \tag{3}$$

where

- Δf amplifier frequency bandwidth;
- A detector area;
- ΔV_n total noise voltage of the system.

The voltage noise includes Johnson noise due to the thermal agitation of charge carriers, and $1/f$-noise observed in low frequencies, usually due to trapping and detrapping mechanisms and surface state scattering. In addition, there is temperature fluctuation noise arising from the fluctuations in the heat exchange between the isolated sensor and its heat sink. The noise component with the lowest magnitude is a fundamental noise referred to as the background noise. The background noise results from the blackbody radiative exchange between the detector and the ambient background and represents the lowest attainable noise level.

The power-normalized $1/f$-noise corner frequency is used to make quantitative comparison between different microbolometer materials since it provides a measure of the inherent noise in the thermometer material. The power normalized $1/f$-noise corner frequency is determined by the frequency at which the Johnson noise equals the $1/f$-noise given by the Hooge equation [17]

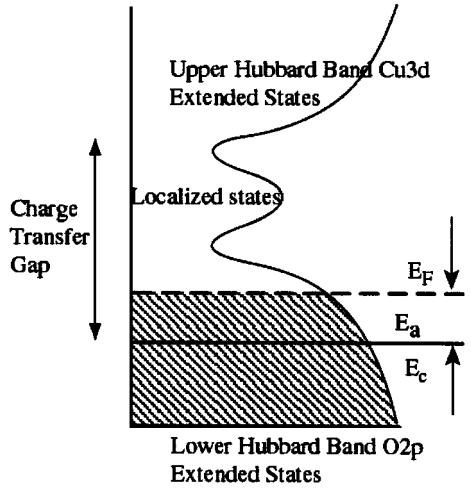

Fig. 1. Schematic of semiconductor-like Fermi glass according to the Yu and Heeger model.

$$\frac{\Delta V_n^2}{\Delta f} = \frac{\alpha_H I_b^2 R^2}{f_c N} = 4kTR \tag{4a}$$

$$\frac{f_c}{I_b^2 R} = \frac{\alpha_H}{4kTN} = \frac{1}{4kT}\left(\frac{\Delta V_n}{I_b R}\right)^2 \frac{f}{\Delta f}. \tag{4b}$$

Here, f_c is the $1/f$-noise corner frequency, α_H is Hooge's coefficient, N is the number of fluctuators in the sample. A microbolometer must have large values of β, R_v, and D^* for good performance.

Recently, $YBa_2Cu_3O_{6+x}$ has been investigated as an uncooled microbolometer and a pyroelectric detector. The electrical and optical properties of $YBa_2Cu_3O_{6+x}$ vary with the oxygen stoichiometry. At ($0 \leq x \leq 0.3$), the Y–Ba–Cu–O compound is a Mott-Hubbard insulator with a well-defined energy charge transfer gap of approximately 1.5 eV present between the O (2p) band and Cu (3d) band. The crystal structure is tetragonal when all O1 sites are vacant. As x is increased ($0.3 < x < 0.5$), random oxygen doping introduces disorder to O1 sites of the intercalated layers, producing localized states that serve as charge reservoirs for the transfer of carriers to the conduction planes. Thus, Y–Ba–Cu–O displays the electronic characteristics of a Fermi glass (Fig. 1). As x is increased above ($x \geq 0.5$), Y–Ba–Cu–O undergoes a semiconductor-metal transition to metallic state with an orthorhombic structure that exhibits superconductivity upon cooling to cryogenic temperatures [18]. Y–Ba–Cu–O is best known as a high temperature superconductor ($x \sim 1$). Several groups have investigated superconductive microbolometers measuring detectivities as high as 6×10^9 cm $Hz^{1/2}$/W [19]–[22]. However, the cost of refrigeration and the requirement for high deposition temperatures to achieve proper oxygen stoichiometry with oriented epitaxial growth limit the application of high-T_c superconductor bolometers.

In this work, the semiconducting phase of Y–Ba–Cu–O is used. It is polycrystalline to amorphous and therefore can be deposited on a variety of substrates at ambient temperature [23]–[25]. The TCR is negative with a magnitude of 3.1–3.5%/K observed over a large temperature range near room temperature [26], [27]. Another alternative for room temperature bolometric material is vanadium oxide, which is extensively used in current microbolometer cameras [16], [28]–[31]. VO_x thin films that are typically employed in microbolometer arrays, have a TCR of ∼2%/K at 25 °C, with a relatively low $1/f$-noise, and optical properties that allow high microbolometer IR absorption. Thin-film VO_2 operated at the 68 °C phase-transition temperature undergoes a three-decade change in resistance, while changing into a metallic phase. This transition, however, has latent heat, which degrades the benefits of the high TCR. In addition, the metallic phase is highly reflective. There are also fabrication difficulties, regarding deposition of the desired phase, which is challenging due to the narrow range of oxide stability. Another bolometer material, amorphous silicon, requires low-stress layers, which are obtained by high-temperature annealing. However, with this fabrication method, the advantage of post-CMOS compatibility is lost. a : Si has a TCR similar to VO_x, but higher $1/f$ noise [31], [32].

Y–Ba–Cu–O microbolometers have gone through an evolution of three generations. In the first generation, the thermal isolation structure was bulk-micromachined by thermally growing 15 000-Å-thick SiO_2-bridge on Si without using sacrificial layers. These detectors achieved high responsivities and detectivities, over 10^4 V/W, and 9.45×10^7 cm $Hz^{1/2}$/W, respectively. The TCR was −3.5%/K, but the thermal conductivity and thermal capacitance were fairly high 8×10^{-6} W/K, and 4.6×10^{-9} J/K, respectively, due to the thickness of the microbridge structure [23], [33], [34]. The second generation of microbolometers was processed employing a micromachined Si_3N_4 membrane and a sputtered MgO film as the sacrificial layer. These detectors displayed a detectivity of 1.08×10^8 cm $Hz^{1/2}$/W. The thermal conductance in vacuum and thermal mass of this structure were measured to be $G = 5 \times 10^{-7}$ W/K and $C = 2.6 \times 10^{-9}$ J/K respectively. This corresponds to a thermal time constant of 5.2-ms.

The ability to deposit Y–Ba–Cu–O on a variety of substrates and to micromachine the material is extended in this work to fabricate thermal isolation structures that eliminate the need for a supporting membrane. In this case, the semiconducting Y–Ba–Cu–O is deposited directly on a polyimide sacrificial layer, which is removed to produce free-standing or self-supporting Y–Ba–Cu–O structure. The Y–Ba–Cu–O is held above the substrate only by the electrode arms without the need of any underlying supporting membrane. This represents a simplification of the fabrication procedure for a microbolometer pixel and also represents a significant improvement in the state-of-art for microbolometers by eliminating the thermal mass of the supporting membrane. The reduced thermal mass allows for reducing the thermal conductance to the substrate and thereby increased responsivity and detectivity or having a shorter thermal time constant with the same thermal conductance.

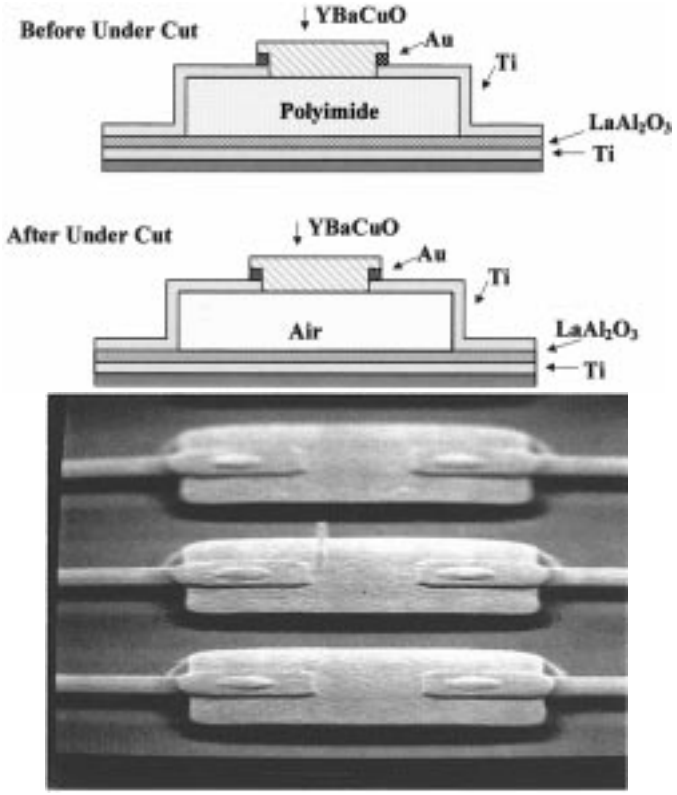

Fig. 2. Self-supporting Y–Ba–Cu–O microbolometer geometry before and after the undercut procedure. 1 × 10 arrays were fabricated with 40 μm × 40 μm pixel size. SEM micrograph of the resulting devices.

II. Fabrication Procedure

The Y–Ba–Cu–O microbolometers investigated in this paper were fabricated using conventional polyimide sacrificial layer and no supporting membrane for the Y–Ba–Cu–O thermometer. The microbolometers were fabricated in 1 × 10 arrays of square pixels, each measuring 40 μm on a side and two electrodes arms 32-μm long. The two device geometries are shown schematically before etching and after etching the sacrificial layer along with a SEM micrograph in Fig. 2. The general device fabrication procedure follows. A four-target, cryo-pumped, CVC601 sputter system was used for all sputter depositions. The <111> n-type 5–15 Ω cm silicon wafer was covered by thick titanium metal mirror, deposited by RF magnetron sputtering at 150 watt in pure argon environment at 10 mTorr pressure. The nominal thickness of Ti was 300 nm. The titanium film was then exposed to O_2 by placing the wafer in a plasma etching system for 10 minutes. This procedure oxidized the surface of the Ti and improved the adhesion of $LaAl_2O_3$, which serves to electrically isolate the electrode arm from the continuous mirror. The thick Ti is a highly reflecting material, forming a resonant cavity with the Y–Ba–Cu–O thermometer. The continuous mirror prevents the excitation of electron-hole pairs in the substrate. Next, 300 nm of insulating material, $LaAl_2O_3$ was deposited by RF magnetron sputtering in pure argon environment at 100 watt rf power. The $LaAl_2O_3$ was chosen because it has low IR absorption. The wafer was then coated with Dupont polyimide (PI2610) and soft baked for 40 min at 140 °C. The polyimide was subsequently cured at 270 °C in N_2 environment to obtain

a durable film, nominally 1.7 μm thick. The polyimide was then patterned into rectangular mesas using standard photolithography and etching with O_2 plasma.

The electrode arms and Au contacts were deposited by sequential RF magnetron sputtering. The nominal thickness of Ti electrode and Au contacts were 100 nm and 40 nm, respectively. Gold was patterned by wet etching with a KI–I_2 solution. Then titanium layer was patterned with a CF_4 dry plasma etch. The two-metal-electrode was employed since metals such as Au, Pt, or Ag make the best electrical contact to Y–Ba–Cu–O. Ti makes a highly resistive contact to Y–Ba–Cu–O but has a relatively low thermal conductivity (0.219 W/cm K) and therefore provides better thermal isolation than if a single, high thermal conductivity metal such as Au (3.1 W/cm K), Pt (0.716 W/cm K), or Ag (4.29 W/ cm K) were used. Different contact sizes varying from 35×10 μm^2 to 10×10 μm^2 were used to explore the effect of contact size on detector noise.

The semiconducting Y–Ba–Cu–O thermometer layer was then deposited by RF magnetron sputtering at ambient temperature in 10 mTorr of Ar. The Y–Ba–Cu–O pixel was patterned using conventional photolithography and wet etching with 1 : 100 Al-etch composition. The nominal thickness was 400 nm. Next, the polyimide mesa was removed by ashing for 3–4 h to suspend the Y–Ba–Cu–O pixel and form the thermal isolation structure. In earlier devices, it was found that the microbolometers that underwent a continuous polyimide undercut etch failed due to cracking when current biased. By interrupting the undercut etch procedure every 30 minutes, the stress-cracking problem was eliminated. It is believed that the induced thermal stress resulting from the continuous exposure to oxygen plasma had caused the Y–Ba–Cu–O microbolometers to fail. The earlier devices used Nb as the electrode arms, which put the device under stress, leading to bowing of the microbolometer. Ti does not appear to place the thermometer under stress.

The gap between the reflecting mirror and the semiconducting Y–Ba–Cu–O was designed to produce a $1/4$-wave resonant cavity between the upper level and the underlying reflector for wavelength near 10 μm.

III. Measurements and Results

The two-probe electrical resistance was mapped out by taking measurements on specified die from the center to the periphery of the wafer. Both polarities were measured. Devices named MM1 and MM2, described here, display representative characteristics of microbolometers fabricated in this manner, utilized 10×10 μm^2 and 10×35 μm^2 Au contacts to the Y–Ba–Cu–O thermometer, respectively. The two-probe resistance for devices like MM1 ranged from 0.8 to 1.2 MΩ at room temperature. The two-probe resistance of MM2 was 0.55 MΩ. These devices show linear I–V characteristics up to 2 μA with no evidence of joule heating.

The measurements of resistance versus temperature ($R-T$), TCR and current–voltage (I–V) characteristics were performed by mounting the devices in a Leybold ROK 10–300 K closed-cycle cryostat refrigerator evacuated to 50 mtorr. A Hewlett-Packard 4142B Modular DC Source/Monitor unit was utilized to measure the I–V characteristics. Hewlett-Packard multimeters were used to measure the resistance of the devices. The resistance versus temperature, the corresponding TCR versus temperature, and I–V characteristics are shown in Fig. 3. The two probe TCR was measured on these three devices from 240 to 320 K and had value of about 3.1%K^{-1} at 296 K. This is somewhat lower in magnitude than the previously measured values of 3.5%K^{-1} on similar Y–Ba–Cu–O samples [25], [33]. The small difference can be attributed to the exposure of Y–Ba–Cu–O to the oxygen plasma during the polyimide mesa ashing to form the suspended structure, and sputtering Y–Ba–Cu–O at a lower power. Increased oxygen concentration in Y–Ba–Cu–O provides more hole carriers and lower resistivity. The thermal conductance of the self-supporting bolometers was measured by the method of resistive or Joule heating at different substrate temperatures. The following relation was employed to calculate G:

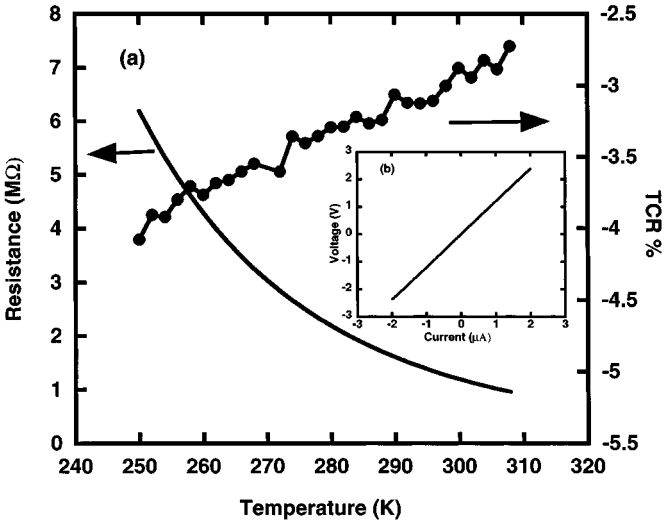

Fig. 3. (a) Resistance and TCR versus temperature and (b) Current–voltage characteristics for device MM1.

$$R(T) = R_0 + \frac{1}{G} \cdot \frac{dR}{dT} I_b^2 R(T). \tag{5}$$

Here, R_o and $R(T)$ are the resistance values at low and high bias currents, respectively. The dR/dT is known from the R–T measurements. It was also measured again with Hewlett-Packard 4142B Modular DC source/Monitor unit at a constant current of 2 μA (high bias). The resistance measured at different currents ranging up to 2 μA and two different polarities was plotted versus dissipated power at a constant substrate temperature. The thermal conductance, G, was calculated from the slope of this characteristic. The room temperature values of G were 1.9×10^{-6} W/K for device MM1 and 2.2×10^{-6} W/K for MM2. The devices have similar G values since the electrode arms were fabricated with the same nominal thickness.

The optical response of the devices was measured by using Oriel 60 071 light source housing a 6575-IR ceramic element, and 60 077 ZnSe condenser/collimator and optical long pass filter LP2500. The radiating element can be modeled as a 1450 K blackbody source. The net usable range of this

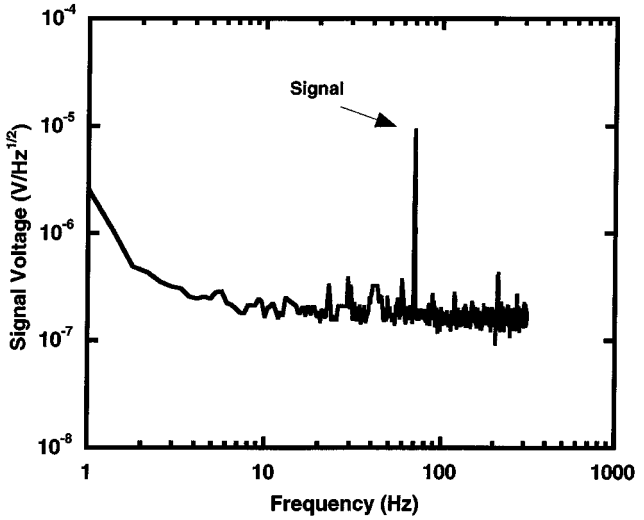

Fig. 4. Typical voltage signal spectrum measured by the dynamic signal analyzer across the microbolometer in response to broad-band IR radiation chopped at 70 Hz. The signal was measured in air with a current bias of 0.41 μA.

broadband system was $\sim$0.6–13 μm. The optical power of the broadband source was approximately 10 mW/cm^2. The long-pass optical filter restricted the optical band to 2.5–13 μm with an irradiance of 5 mW/cm^2. The room temperature measurements were performed in air inside an electromagnetically shielded room. The devices were mounted on an XYZ stage placed inside a shielded box with an aperture in front of the device, allowing the mechanically chopped light to fully illuminate the sample surface. At this time, no window material was used. The vacuum measurements were performed in a cryostat through a ZnSe window. In this case, the irradiance in the 0.6-to-13-μm and 2.5-to-13-μm bands were approximately 0.5 mW/cm^2 and 0.14 mW/cm^2, respectively. The devices were connected to a PAR113 preamplifier and a Hewlett-Packard 3562A dynamic signal analyzer. A dc bias was applied varying from 0.23 to 1.40 μA, supplied by a low-noise, battery-powered current source. The signal analyzer simultaneously measured the signal amplitude and noise per unit bandwidth for each chopper frequency. The response was calibrated with an Oriel 70 124 pyroelectric detector. A typical voltage spectrum in vacuum at bias current $I_b = 0.41$ μA is shown in Fig. 4 with the broad-band IR source chopped at 70 Hz. The figure displays a strong voltage response at the chopper frequency. At 70 Hz, the Johnson noise of the Y–Ba–Cu–O thermometer determined the noise voltage. At frequencies less than 10 Hz, $1/f$-noise arises. The power normalized corner frequency (f_c/I_b^2R) was calculated to be 45 Hz/μW and 35 Hz/μW at 0.41 μA of current bias for devices MM1 and MM2, respectively. The corner frequencies reported here are slightly higher than the 25 Hz/μW reported earlier on Y–Ba–Cu–O [35]. The difference in the power normalized corner frequency between the representative data on the self-supporting Y–Ba–Cu–O structures and the Y–Ba–Cu–O devices in [35] is not considered statistically significant. The authors have not observed a dependence of the $1/f$-noise on the volume of the Y–Ba–Cu–O film or the contact area. This would appear to rule out bulk and contact fluctuators as sources of $1/f$-noise. Power normalized corner frequencies

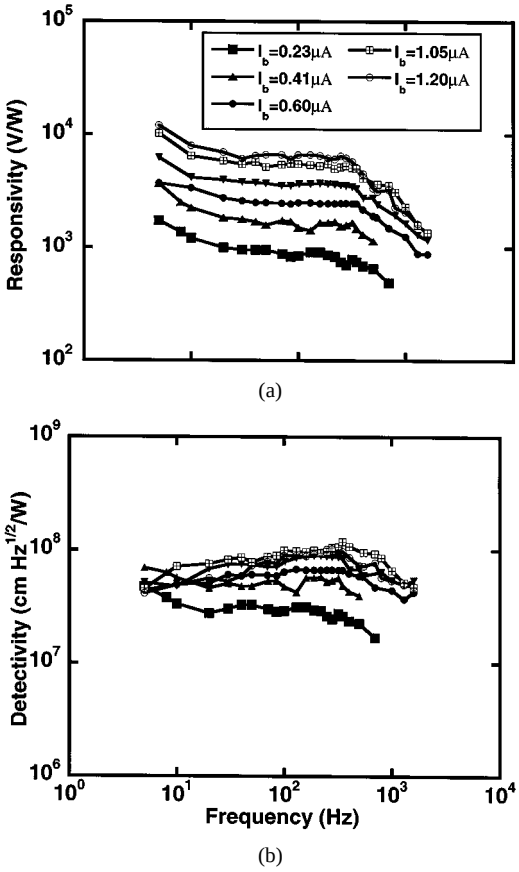

Fig. 5. Responsivity (a) and detectivity (b) as a function of chopper frequency at different current biases measured in vacuum with 2.5 to 13 μm broad-band IR radiation.

as low as 0.2 to 2 Hz/μW have been observed in Y–Ba–Cu–O microbolometers using Si_3N_4 encapsulation and 4.65 μA of current bias [36]. However, as in the earlier investigations, it is unclear whether the $1/f$-noise arises from the Y–Ba–Cu–O thermometer or is instrumentation related. If one compares these values to other uncooled IR sensing materials, the power normalized corner frequency is 8 Hz/μW [32] and 250 Hz/μW [32] for VO_x and a : Si bolometers, respectively.

The responsivity and detectivity were measured both in air and vacuum at room temperature. The responsivity displayed about a factor of 8 improvement with the evacuation of the cryostat. The small improvement results from the relatively high thermal conductance of the electrode arms, which are 10 μm wide, 32 μm long and 100 nm thick. The vacuum responsivity and detectivity of device MM1 are plotted as a function of chopper frequency at different bias currents for device MM1 in Fig. 5. In vacuum, responsivity as high as 7.95 $\times$ 10^3 V/W was measured. The highest measured detectivity was 1.19 $\times$ 10^8 cm Hz$^{1/2}$/W at bias current $I_b = 1.05$ μA. For comparison, the responsivity and detectivity of device MM2 at bias current of 0.88 μA was 1.88 $\times$ 10^3 V/W, and 5.87 $\times$ 10^7 cm Hz$^{1/2}$/W, respectively. The responsivity and detectivity at the same current value for MM1 was 4.16 $\times$ 10^3 V/W and 8.92 $\times$ 10^7 cm Hz$^{1/2}$/W. The reason for having lower responsivities and detectivities in device MM2 is the decrease in resistance. The decrease in responsivity at high chopper frequencies is due to the thermal time constant of the microbolometer.

TABLE I
SUMMARY OF MICROBOLOMETER PROPERTIES

	Device MM1	Device MM2	**1st generation bolometer**
Description	Surface micromachined using polyimide sacrificial layer and self-supporting Y-Ba-Cu-O bridge		Bulk Micromachined SiO_2 bridge, using isotropic etch
Y-Ba-Cu-O thickness $t_{\mu m}$ (nm)	400	400	200
Ti-electrode thickness t_{ea} (nm)	100	100	200
Au contact thickness t_c (nm)	40	40	300
Contact area (μm) $W_c \times L_c$	10×10	10×35	12×14
2- Wire resistance at 295 K (MΩ)	1	0.5	7.8
TCR (%K)	3.1	3	3.5
Thermal conductivity G_{th}(W/K)	1.9×10^{-6}	2.2×10^{-6}	8×10^{-6}
Absorption η (%)	30	37	27 %
Thermal capacitance C (J/K)	3.53×10^{-10}	4.2×10^{-10}	$4.2\text{-}4.6\times10^{-9}$
Thermal time constant, τ_{th} (ms)	0.17-0.22	~0.20	0.53-0.58
Maximum responsivity R_V (V/W)	7.95×10^{3} @ 1.05 μA	1.88×10^{3} @ 0.9 μA	1.92×10^{4} @ 1.5 μA
Maximum detectivity D^*(cm $Hz^{1/2}$/W)	1.19×10^{8} @1.05 μA	5.87×10^{7} @ 0.9 μA	9.45×10^{7} @ 1.5 μA
Power normalized 1/f noise corner frequency (Hz/μW)	45 @ 0.41 μA	35 @ 1.0 μA	25 @ 0.41 μA

By fitting the responsivity data for MM1 and MM2 to (5), the values of G/η were calculated to be 6.5×10^{-6} W/K and 5.6×10^{-6} W/K respectively. The thermal time constant, τ_{th} ranged between 0.17–0.22 ms, resulting in thermal mass, C, 3.5×10^{-10} J/K and 4.2×10^{-10} J/K. This represents approximately one order of magnitude lower thermal mass than obtained in our previous microbolometer structures, mainly due to the elimination of the supporting membrane. The C value obtained here is also much smaller than that reported in conjunction with VO_x, Pt and Poly-Si–Ge microbolometers [8], [12], [13], [15], [16]. The absorptivity was calculated to be 30% for MM1 and 37% for MM2 from the fitted G/η value and the G measured by Joule heating. This represents a relatively strong IR absorption for the freestanding YBCO thermometer, especially considering the fact that no absorber layer was utilized. A summary of the measured and fitted data for the two devices is presented in Table I.

The thermal mass of the microbolometer structure can be estimated from the specific heat capacity and the volume of the individual component making up the microbridge, namely: the IR sensitive layer (subscript μb); Au contacts (subscript c); and Ti electrode arms (subscript ea)

$$C = W_{\mu b} L_{\mu b} t_{\mu b} c_{YBCO} + 2 W_c L_c t_c c_{Au} + 2\left(\tfrac{1}{3} W_{ea} L_{ea} t_{ea} c_{Ti}\right). \quad (6)$$

Here, W, L, and t correspond to width, length, and thickness of each component. Since the electrode arms make contact with the substrate, only one-third contribution is assumed from each arm. This yields an approximate C of 1×10^{-9} J/K, which is higher than the measured value. The discrepancy might be partly due to the overetching of the IR sensitive layer, thus yielding a lower overall mass and hence measured thermal capacitance. The specific heat of Y–Ba–Cu–O, Au and Ti are comparable (2.65, 2.47 and 2.34 J/K-cm^3, respectively). However, due to the relatively high mass of the Y–Ba–Cu–O layer, the total thermal capacitance is mostly determined by this layer.

The noise equivalent temperature difference (NETD) is a system figure of merit defined as

$$\text{NETD} = \frac{4F^2\Delta V_n}{\tau_0 A R_V (\Delta P/\Delta T)_{\lambda_1-\lambda_2}} \tag{7}$$

where, F is the focal ratio of the optics, τ_0 is the transmittance of the optics, and $(\Delta P/\Delta T)\lambda_1 - \lambda_2$is the change in optical power with respect to temperature per unit area radiated by a blackbody at temperature T, measured within the spectral band from λ_1 to λ_2. For a blackbody at 295 K, $(\Delta P/\Delta T)_{\lambda_1-\lambda_2}$ is 2.62×10^{-4} W/cm^2 K in 8–14 μm spectral interval [4]. Assuming the detectivity in the 8–14 μm window to be the same as measured over the 2.5–13 μm band, F/1 optics, $\tau_o = 1$ and an electrical bandwidth of 4 Hz for the preamplifier, (7) yields an NETD of 65 mK for detector MM2 at 0.88 μA of bias. Therefore, NETD less than 100 mK is achievable with some latitude in the system parameters.

IV. Conclusion

Self-supporting Y–Ba–Cu–O thermal detectors have been fabricated using a conventional polyimide sacrificial layer technology and ashing in oxygen plasma. No additional supporting membrane is required to support Y–Ba–Cu–O pixel. The process for self-supporting Y–Ba–Cu–O is considerably simpler than that employed in conventional microbolometers and can be used in conjunction with CMOS technology to produce focal plane arrays. The microbolometers displayed responsivity and detectivity as high as 7.95×10^3 V/W and 1.19×10^8 cm Hz$^{1/2}$/W. Y–Ba–Cu–O showed much lower normalized $1/f$ corner than amorphous silicon but higher than VO_x by a factor of 4 to 6. The self-supporting structure resulted in an order of magnitude reduction in thermal mass (3.52×10^{-10}J/K). This reduction in thermal mass allows for higher thermal cutoff frequencies that would be useful in high-speed cameras or may be traded-off with the thermal conductance to produce higher responsivity and detectivity of the microbolometer. The Y–Ba–Cu–O displays good absorptivity characteristics (30%) in the 2.5 to 13 μm band. The exposure of Y–Ba–Cu–O thermometer to the oxygen plasma during the undercut etch is believed to have resulted in a slight reduction of the TCR of the thermometer to -3%/K. In future, passivating the Y–Ba–Cu–O thermometers with thin dielectric coatings will be investigated. The effect of the passivation on the TCR and $1/f$-noise will also be studied. A thin metal film absorber will be incorporated into the structure to improve the absorptivity. Finally, the self-supporting Y–Ba–Cu–O uncooled detector structure opens the door for the investigation of the Y–Ba–Cu–O IR characteristics without any additional interference from a supporting membrane or substrate.

Acknowledgment

The authors would like to thank the Cornell Nanofabrication facility for fabricating the photolithography masks used to fabricate the device structures. The authors would also like to thank N. Amarasinghe for his help in bonding the devices.

References

[1] C. Marshall, N. Butler, R. Blackwell, R. Murphy, and T. Breen, "Uncooled infrared sensor with digital focal plane array," *SPIE*, vol. 2746, p. 23, 1996.

[2] T. White, N. Butler, and R. Murphy, "An uncooled IR sensor with digital focal plane array," *IEEE Eng. Med. Biol.*, p. 60, 1998.

[3] R. A. Wood and N. A. Foss, "Micromachined bolometer arrays achieve low-cost imaging," *Laser Focus World*, p. 101, 1993.

[4] P. W. Kruse, "Principles of uncooled infrared focal plane arrays," in *Uncooled Infrared Imaging Arrays and Systems*, P. W. Kruse and D. D. Skatrud, Eds. New York: Academic, 1997, vol. 47, in Semiconductors and Semimetals.

[5] ——, "A comparison of the limits to the performance of thermal and photon detector imaging arrays," *Infrared Phys. Technol.*, vol. 36, p. 869, 1995.

[6] J. F. Belcher, C. M. Hanson, H. R. Beratan, K. R. Udayakumar, and K. L. Soch, "Uncooled Monolithic Ferroelectric IRFPA Technology," *SPIE*, vol. 3436, p. 611, 1998.

[7] B. Cole, R. Horning, B. Johnson, K. Nguyen, P. W. Kruse, and M. C. Foote, "High performance infrared detector array using thin film microstructures," in *Proc. 9th IEEE Int. Symp. Application of Ferroelectric*, 1994, p. 653.

[8] W. Radford, R. Wyles, J. Wyles, J. Varesi, M. Ray, D. Murphy, A. Kennedy, A. Finch, E. Moody, F. Cheung, R. Coda, and S. Baur, "Microbolometer uncooled infrared camera with 20 mK NETD," *SPIE*, vol. 3436, p. 636, 1998.

[9] Z. Çelik-Butler and D. P. Butler, "Uncooled infrared detector arrays," in *Wiley Encyclopedia of Electrical and Electronics Engineering*. New York: Wiley, 1999, vol. 10, p. 198.

[10] A. Tanaka, S. Matsumoto, N. Tsukamoto, and N. Teranishi, "Silicon IC process compatible bolometer infrared focal plane array," in *Proc. 8th International Conference on Solid-State Sensors Actuators, Eurosensors IX*, Stockholm, Sweden, June 25–29, 1995.

[11] H. Lee, J. Yoon, E. Yoon, S. Ju, Y. Yong, W. Lee, and S. Kim, "A high fill-factor IR bolometer using multi-level electrothermal structures," in *Proc. IEEE International Electron Devices Meeting*, 1998, p. 463.

[12] J. Wauters, "Doped silicon creates new bolometer material," *Laser Focus World*, p. 145, 1997.

[13] S. Sedky, P. Fiorini, K. Baert, L. Hermans, and R. Mertens, "Characterization and optimization of infrared poly SiGe bolometers," *IEEE Trans. Electron Devices*, vol. 46, p. 675, 1999.

[14] L. Boarino, G. Lerondel, E. Monticone, R. Steni, G. Amato, G. Benedetto, V. Lacquaniti, and R. Spagnolo, "Design and fabrication of metal bolometers on high porosity silicon layers," in *Proc. 4th THERMINIC Workshop*: Cannes, Sept. 27–29, 1998.

[15] P. Eriksson, J. Y. Andersson, and G. Stemme, "Thermal characterization of surface-micromachined silicon nitride membranes for thermal infrared detectors," *J. Microelectromechan. Syst.*, vol. 6, p. 55, 1997.

[16] W. Radford, D. Murphy, M. Ray, S. Propst, A. Kennedy, J. Kojiro, J. Woolaway, K. Soch, R. Coda, G. Lung, E. Moody, D. Gleichman, and S. Baur, "320×240 silicon microbolometer uncooled IRFPA's with on-chip offset correction," *SPIE*, vol. 2746, p. 82, 1996.

[17] F. N. Hooge, "$1/f$ noise is no surface effect," *Phys. Lett.*, vol. 29A, p. 139, 1969.

[18] G. Yu and A. J. Heeger, "Photoinduced charge carriers in insulating cuprates: Fermi glass insulator, metal-insulator transition and superconductivity," *Int. J. Modern Phys. B*, vol. 7, p. 3751, 1993.

[19] J. C. Brasunas and B. Lakew, "High T_c superconductor bolometer with record performance," *Appl. Phys. Lett.*, vol. 64, p. 777, 1994.

[20] M. Nahum, Q. Hu, P. L. Richards, S. A. Sachtjen, N. Newman, and B. F. Cole, "Fabrication and measurement of high T_c superconducting microbolometers," *IEEE Trans. Magn.*, vol. MAG-27, p. 3081, 1991.

[21] B. R. Johnson, T. Ohnstein, C. J. Han, R. Higashi, P. W. Kruse, R. A. Wood, H. Marsh, and S. B. Dunham, "$YBa_2Cu_3O_7$ superconducting microbolometer arrays fabricated by silicon micromachining," *IEEE Trans. Appl. Superconduct.*, vol. 3, p. 2856, 1993.

[22] T. G. Stratton, B. E. Cole, P. W. Kruse, R. A. Wood, K. Beauchamp, T. F. Wang, B. Johnson, and A. M. Goldman, "High-temperature superconducting microbolometer," *Appl. Phys. Lett.*, vol. 57, p. 99, 1990.

[23] D. P. Butler, Z. Çelik-Butler, A. Jahanzeb, J. E. Gray, and C. M. Travers, "Micromachined YBaCuO capacitor structures as uncooled pyroelectric infrared detectors," *J. Appl. Phys.*, vol. 84, p. 1680, 1998.

[24] Z. Çelik-Butler, P. C. Shan, D. P. Butler, A. Jahanzeb, C. M Travers, W. Kula, and R. Sobolewski, "Charge transport in amorphous and tetragonal semiconducting YBaCuO films," *Solid-State Electron.*, vol. 41, p. 895, 1997.
[25] P. C. Shan, Z. Çelik-Butler, D. P. Butler, A. Jahanzeb, C. M Travers, W. Kula, and R. Sobolewski, "Investigation of semiconducting Y–Ba–Cu–O thin films: A new room temperature bolometer," *J. Appl. Phys.*, vol. 80, p. 7118, 1996.
[26] M. Almasri, D. P. Butler, and Z. Çelik-Butler, "Free standing amorphous Y–Ba–Cu–O detectors for uncooled IR detection and the effects of doping," *SPIE*, vol. 3794, p. 66, 1999.
[27] ——, "Semiconducting YBCO bolometers for uncooled IR detection," *SPIE*, vol. 4028, Infrared Detectors and Focal Plane Arrays VI, p. 17, 2000.
[28] B. E. Cole, R. E. Higashi, and R. A. Wood, "Monolithic arrays of micromachined pixels for infrared application," in *Proc. IEEE International Electron Devices Meeting*, 1998, p. 459.
[29] T. Breen, N. Butler, M. Kohin, C. A. Marshall, R. Murphy, T. Parker, and R. Silva, "More applications of uncooled microbolometer sensors," *SPIE*, vol. 3436, p. 530, 1998.
[30] B. Meyer, R. Cannata, A. Stout, A. Gin, and P. Taylor, "Amber's uncooled microbolometer LWIR camera," *SPIE*, vol. 2746, p. 13, 1996.
[31] R. A. Wood, "Monolithic silicon microbolometer arrays," in *Uncooled Infrared Imaging Arrays and Systems*, P. W. Kruse and D. D. Skatrud, Eds. New York: Academic, 1997, vol. 47, in Semiconductors and Semimetals.
[32] B. I. Craig, R. J. Watson, and M. H. Unewisse, "Anisotropic excess noise within a-Si : H," *Solid-State Electron.*, vol. 39, p. 807, 1996.
[33] C. M. Travers, A. Jahanzeb, D. P. Butler, and Z. Çelik-Butler, "Fabrication of semiconducting YBaCuO surface-micromachined bolometer arrays," *J. Microelectromechan. Syst.*, vol. 6, p. 271, 1997.
[34] J. E. Gray, Z. Çelik-Butler, D. P. Butler, and A. Jahanzeb, "Uncooled infrared microbolometers and pyroelectric detectors using semiconducting YBaCuO," *SPIE*, vol. 3436, p. 555, 1998.
[35] J. Gray, Z. Çelik-Butler, D. P. Butler, and M. Almasri, "Semiconducting YBaCuO as infrared detecting bolometers," *SPIE*, vol. 3436, p. 555, 1998.
[36] M. Almasri, Z. Çelik-Butler, D. P. Butler, A. Yaradanakul, and A. Yildez, "Semiconducting YBaCuO microbolometers for uncooled broad-band IR sensing," in Proceedings of the SPIE Aerosense, Infrared Technology and Applications XXVII, Orlando, FL, Apr. 2001.

Mahmoud Almasri (S'00) received the B.Sc. and M.Sc. degrees in physics from Bogazici University, Istanbul, Turkey, in 1995 and 1997, respectively. He is currently working toward the Ph.D. degree in electrical engineering at Southern Methodist University, Dallas, TX.

His research interests include fabrication and electrical, optical, and dielectric characterization of uncooled infrared detectors. He coauthored six conference and journal papers in these areas.

Mr. Almasri was awarded the Southern Methodist University, "Frederick E. Terman Award," in Electrical Engineering in 1999–2000. He is a student member of SPIE.

Donald P. Butler (S'80–M'87–SM'98) received the B.A.Sc. degree in engineering science with a physics option from the University of Toronto, Toronto, ON, Canada, in 1980 and the M.S. and Ph.D. degrees in electrical engineering from the University of Rochester, Rochester, NY, in 1981 and 1986, respectively.

He performed his graduate research at the Laboratory for Laser Energetics investigating the nonequilibrium behavior of superconductor thin films in response to picosecond electrical and optical excitations. He continued his graduate research as a research associate in 1986. In 1987, he joined the Electrical Engineering at Southern Methodist University (SMU), Dallas, TX, as an Assistant Professor. In 1993, he was promoted to the rank of Associate Professor. While at SMU, he has been involved in research projects involving the optical control of superconductive microwave transmission line filters, the investigation of high-temperature superconductors for hybrid superconductor-semiconductor electronics, the application of high temperature superconductors to microwave mixing and parametric conversion, the characterization of GaAs MMIC's at cryogenic temperatures, the investigation of GaAs HBTs at cryogenic temperatures and uncooled infrared imaging. His current research involves materials and devices for uncooled infrared detection and microelectromechanical devices. He holds four patents and he authored over 130 publications, and he has three books and book chapter. His work has been supported by Texas Higher education coordinating Board Advanced Technology program, the National Science Foundation, E-systems, Hewlett-Packard, Army Research Office, NASA-Langeley, and the IEEE microwave Theory and Techniques society.

Dr. Butler is a member of the American Physical Society, member of SPIE, and member of American society for engineering education.

Zeynep Çelik-Butler (S'80–M'87–SM'98) received the dual B.S. degrees in electrical engineering and physics from Bogaziçi University, Istanbul, Turkey, in 1982. She received the M.S. and Ph.D. degrees in electrical engineering from the University of Rochester, Rochester, NY, in 1984 and 1987, respectively.

She was an IBM Predoctoral Fellow from 1983 to 1984, and an Eastman Kodak Predoctoral Fellow from 1985 to 1987. She joined the Department of Electrical Engineering at Southern Methodist University, Dallas, TX, in 1987 as an Assistant Professor; was tenured and promoted to Associate Professor in 1993. She has four patents, two book chapters, and over 85 journal and conference publications in these fields.

Dr. Çelik-Butler was the holder of J. Lindsay Embrey Trustee Assistant Professorship from 1990 to 1993. She served as the Assistant Dean of Graduate Studies and Research from 1996 to 1999. She is currently a Professor of Electrical Engineering. She served in various technical committees including 1988, 1989 IEEE-IEDMs, Annual Symposia on Electronic Materials, Processing and Characterization (1989–1992), and International Conference on Noise in Physical Systems and $1/f$ Fluctuations (1992, 1993, 1997, 2001). She was the General Chair of TEXMEMS II Workshop. She is currently the Technical Editor for Fluctuation and Noise Letters. She has received several awards including the IEEE-Dallas Section Electron Devices Society Outstanding Service Award (1995, 1997), IEEE—Electron Devices Society, Service Recognition Award (1995), Outstanding Electrical Engineering Graduate Faculty Awards (1996, 1997) and Southern Methodist University Sigma Xi Research Award (1997). Her research interests include microelectromechanical systems, infrared detectors, noise in semiconductor and superconductor devices, and high T_c-superconductivity.

Dr. Çelik-Butler is a member of Eta Kappa Nu and the American Physical Society. She is a Distinguished Lecturer for the IEEE—Electron Devices Society.